【Memoirs of Construction Engineering Research Institute Vol.64(papers)Nov.2022】

APPLICATION OF A PARTICLE METHOD TO SIMULATION OF RUNOFF FROM SHORT BUT INTENSE RAINFALL AND STREET FLOODING IN A SMALL CATCHMENT

Sin Ying Tan　Akihiko Nakayama　Xin Yan Lye

ABSTRACT

The runoff from a short-duration rainfall has been simulated using a three-dimensional Smoothed Particle Hydrodynamics (SPH) method developed for simulation of overland flow on natural and urban terrain. The method is based on the three-dimensional weakly-compressible SPH applied to sparsely distributed surface flow due to rainfalls in a small urban catchment at a foot of mountainous terrain. The rainwater is lumped into discrete particles and their infiltration into the ground, the motion of the excess flow and its accumulation are simulated for a real small catchment in Malaysia. The simulation results are compared with the observation of flash flooding of streets. The results for an assumed rainfall are found to show details of surface water movement in agreement with the observation. It can further be refined to simulate overland flow patterns in more general situations.

1. INTRODUCTION

As the global climate is changing the heavy rainfalls and the resulting water hazards are not diminishing. Accurate forecasting of rainfalls, the runoff and possible flooding areas remain as important as ever. The methods and models of rainfall and runoff analyses that have been used are reviewd in various literature (e.g. Sitterson, et al.[1)], Gayathri, et.al.[2)]). Many of them are data-driven models that use statistical correlations between input rainfall and the runoff occurences of the past events (Kokkonen, et al.[3)]). The process of predicting runoffs from rainfall is being improved by making use of recent approach based on machine learning artificial inteligence and deep neural networks but the direct physical processes are not used. It is difficult to predict local phenomena specific to local areas of concern (Beven[4)]). The methods based on physical processes such as the conventional curve number method developed by United States Department of Agriculture Natural Resources Conservation Service (USDA NRCS)[5)] treat the runoffs as lump sums in a cathment or sub catchments and again the detailed local phenomenon is not addressed. The surface flow and inundation simulation based on physical processes can treat individual surface flow but they are two-dimensional (2-d) analyses of Shallow-Water Equations (SWE)[6,7,8)] with simplified hydrostatic approach. Rainfall-runoff-inundation (RRI) model makes use of 2-d diffusive wave equations with infiltration. These models are based on Eulerian fixed grids that cover the area to be simulated and the computation is carried out over the whole area. Recent localized intense rainfalls (e.g. Jamaludin et al.[9)]) that are causing flash floods in short time at specific locations are difficult to be predicted by either of the data-driven method or lumped model analysis.

In recent years, in contrast to the fixed grid methods, meshless methods that treat the motion of indivisual portion of water has been applied to various free surface flow motion. Smoothed Particle Hydrodynamics method, in particular has successfully been applied to various free surface flows[10,11,12)]. These meshless particle interpolation methods have great potential in representing the rainfall itself and the subsequent motion on and in the ground. The 2-dimensional version has been extensively developed and used in overland flow analysis[10,11,12]. However they are still limited to the surface flow only and the flows in channels where the shallow surface need to be analyzed separately by 1-d channel flow analysis[12].

The 3-d SPH method[13,14] on the other hand has been shown to represent the motion of sparsely distributed surface flows as well as ponded patches of water and the channel flows at the same time. The present authors[15,16] have proposed such method and indicated that it can be applied to simulation of the rainfall, runoff, the overland flow, infiltration and the channel flows including stagnant bodies of water. The present work is to apply this method in the simulation of runoff from a rainfall in a real catchment. The observation of a typical rainfall-runoff events has also been made to assess the effectiveness of this new method.

2. WEAKLY COMPRESSIBLE SMOOTHED PARTICLE METHOD APPLIED TO RAINFALL AND DIRECT RUNOFF

2.1 Basic equations of 3d-SPH method

In 3-d SPH methods, the motion of the fluid is represented by the motion of particles that represent the position, the velocity, the pressure of continuous fluid body at discrete points. By giving the volume and the mass of each particle the particle can also be interpreted to represent a lump of fluid. The forms of the equations are the same as those described in Nakayama et al.[15]. The forces acting on these particles are the gravitational force, the pressure force and the viscous forces from surrounding particles and the normal and tangential resistance forces from the solid boundary. Therefore, the equation of particle *a* moving with velocity $\boldsymbol{v}_a$ at time *t* is

$$\frac{d\boldsymbol{v}_a}{dt} = \boldsymbol{g} + \sum_b \boldsymbol{P}_{ab} + \sum_b \boldsymbol{\Pi}_{ab} + \frac{\boldsymbol{T}_w}{\rho_a} \tag{1}$$

where the summation is taken over the neighboring particles *b* that are within the influence distance *h* of 2.3 times the size of the particle, $\boldsymbol{P}_{ab}$ is the pressure force due to particle *b*, Π_{ab} is the viscous force due to particle *b* and $\boldsymbol{T}_w$ is the force due to the solid boundary. The forms of $\boldsymbol{P}_{ab}$ and Π_{ab} are derived from the spatial interpolation of continuous flow and

$$\boldsymbol{P}_{ab} = \left(\frac{p_a}{\rho_a} + \frac{p_b}{\rho_b}\right)\frac{m_b}{\rho_b}\nabla_a W_{ab} \tag{2}$$

$$\boldsymbol{\Pi}_{ab} = \frac{m_b}{\rho_b}\left(\frac{(\mu_a + \mu_{Ta}) + (\mu_b + \mu_{Tb})}{\rho_b \rho_b}\right)(\boldsymbol{v}_a - \boldsymbol{v}_b)\frac{(\boldsymbol{r}_a - \boldsymbol{r}_b)}{|\boldsymbol{r}_a - \boldsymbol{r}_b|^2} \cdot \nabla_a W_{ab} \tag{3}$$

where p_a and p_b are the pressure, ρ_a and ρ_b are the density, μ_a and μ_b are the molecular viscosity, μ_{Ta} and μ_{Tb} are the turbulent viscosity, $\boldsymbol{r}_a$ and $\boldsymbol{r}_b$ are the positions of particles *a* and *b*, respectively, m_b is the mass of particle *b* and $\nabla_a W_{ab}$ is the weight of the forces depended on the distance and the direction of the separation between particles *a* and *b* given by

$$\nabla_a W_{ab} = \begin{cases} -\dfrac{1}{2h}\left[(2-q)^2 - 4(1-q)^2\right]\dfrac{\boldsymbol{r}_a - \boldsymbol{r}_b}{|\boldsymbol{r}_a - \boldsymbol{r}_b|}, 0 \le q \le 1 \\ -\dfrac{1}{2h}(2-q)^2\dfrac{\boldsymbol{r}_a - \boldsymbol{r}_b}{|\boldsymbol{r}_a - \boldsymbol{r}_b|}, 1 \le q \le 2 \\ 0, \quad 2 < q \end{cases} \tag{4}$$

where $q = |\boldsymbol{r}_a - \boldsymbol{r}_b|/h$.

The resistance force $\boldsymbol{T}_w$ from the nearby solid surface is the tangential force in the direction opposite of the particle velocity. If $\boldsymbol{t}$ is the unit vector in the local flow direction, it is expressed as

$$\boldsymbol{T}_w = -C_T \frac{\tau_w}{h_w} \boldsymbol{t} \tag{5}$$

where C_T (=1.0) is an empirical constant h_w is the thickness of the wall layer (taken as $2h$) next to the solid boundary and τ_w is the wall shear stress determined by the wall law

$$\frac{v_t}{u_\tau} = \begin{cases} \mathrm{A} \ln\left(\frac{nu_\tau}{\nu}\right) + B, & 30 < \frac{nu_\tau}{\nu}, \\ \mathrm{C} \ln\left(\frac{nu_\tau}{\nu}\right) + D, & 5 < \frac{nu_\tau}{\nu} < 30, \\ \frac{nu_\tau}{\nu}, & \frac{nu_\tau}{\nu} < 5 \end{cases} \tag{6}$$

where v_t is the tangential velocity of particle a, n is the normal distance from particle a to the boundary, $u_\tau = \sqrt{\tau_w/\rho_a}$, A(=2.5),B(=5.5),C(=5.0) and D(=3.05) are constants and $\nu=\mu_a/\rho_a$, for hydraulically smooth surface with the roughness Reynolds number $R_k = ku_\tau/\nu < 100$ where k is the roughness height. For hydraulically rough surface with $R_k > 100$, the wall law for fully rough surface

$$\frac{v_t}{u_\tau} = \mathrm{A} \ln\left(\frac{n}{k}\right) + E \tag{7}$$

with E=8.5 is used. The density is calculated from the discretized form of the continuity equation with a density diffusion that comes from the turbulent random motion

$$\frac{d\rho_a}{dt} = \sum_b m_b[(\boldsymbol{v}_a - \boldsymbol{v}_b)]\nabla_a W_{ab} + \sum_b m_b[(\boldsymbol{R}_a/\rho_a - \boldsymbol{R}_b/\rho_b)]\nabla_a W_{ab} \tag{8}$$

where $\boldsymbol{R}_a$ and $\boldsymbol{R}_b$ are the density diffusion of particle a and b. The density is assumed to determine the pressure via a state equation

$$p_a = B\left(\left(\frac{\rho_a}{\rho_0}\right)^\gamma - 1\right) \tag{9}$$

with the value of B is chosen so that the speed of sound is 10 times the maximum expected flow velocity at the reference density ρ_0 at the atmospheric pressure and γ=7.

After the velocity $\boldsymbol{v}_a$ is solved the position $\boldsymbol{r}_a$ is determined by

$$\frac{d\boldsymbol{r}_a}{dt} = \boldsymbol{v}_a \tag{10}$$

which complete the basic equations.

The boundary conditions are the zero normal velocity on solid surface except for infiltration. Rather than introducing artificial repulsive force, the normal velocity component is set to zero when the particle comes within the distance h_w from the boundary. The distance to the boundary is obtained by searching for the closest boundary particle which has the information of position and the normal direction as well as the roughness eight and the infiltration capacity. The enforced normal velocity in the wall layer goes in the continuity equation (8) and to automatically increase the density and hence the pressure.

3. SIMULATION AREA AND ITS RUNOFF CHARACTERISTICS

The present rainfall-runoff simulation is applied to a small catchment in a town in Malaysia. It is located in a sub-catchment of a tributary of Perak River in Peninsular Malaysia in Kinta district of Perak State as shown in the red colored area of Fig.1. The focus is on a part of the catchment in a small town of Kampar centered at coordinates 4°19’12”N, 101°8’54”E shown in pink shaded area in Fig.2. It is located at the foot of Gunung Bujung Melaka of the highest elevation of 1234m and is irrigated by Keranji River (Sungai Keranji, Fig.2) and Kampar River (Sungai Kampar, Fig. 2) consisting

Fig.1 location of simulation area in Kinta district in Peninsula Malaysia.

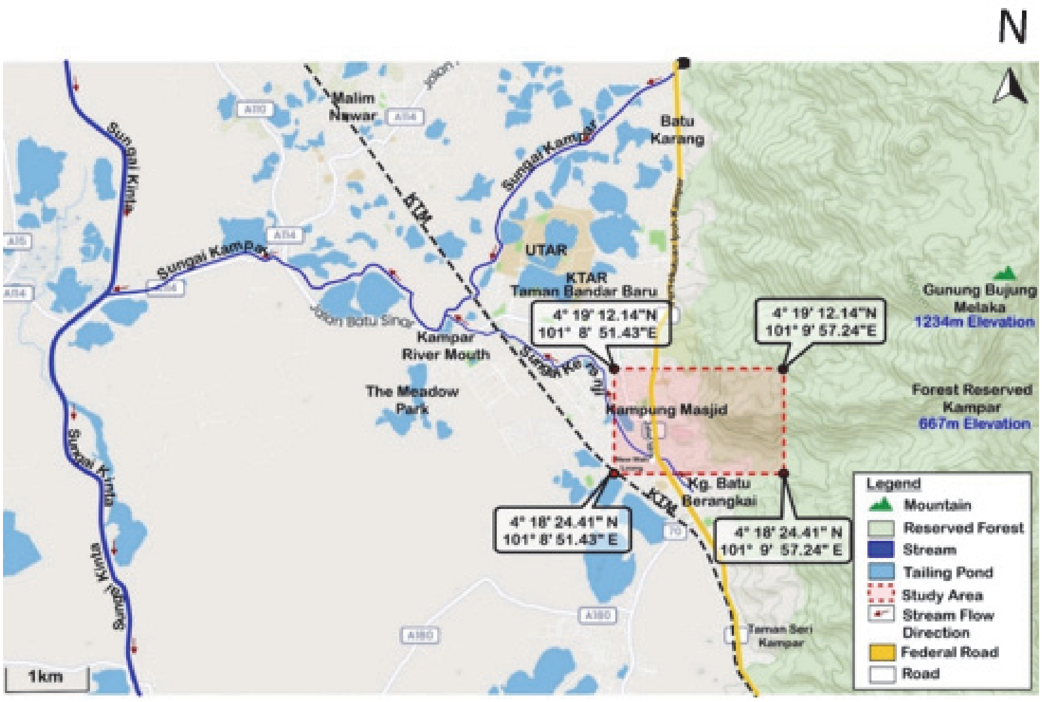

Fig.2 location of Kampar (Kampung Masjid) in Kinta District.

of alluvial soil enriched in tin minerals (Majlis Daerah Kampar[17]). After the decline of the tin mining activities in 1980's, this area is left with tailing ponds that were formed by the ore digging at the low catchment area of Sungai Keranji. The urbanized areas with paved streets nowadays, however, are subjected to frequent flash floodings in rainy seasons. Typical rainfalls that cause street flooding are intense but of relatively short duration of less than one hour. The direct runoff from the mountain side rushes in certain areas called the flood hotspots resulting in more than a foot of water in half an hour. The map in Fig.3 shows some details of the areas of frequent street flooding. Majlis Daerah Kampar[17] started recording the flood prone areas within the Kampar River catchment since 1999. The first area is in front of Maybank Kampar (Fig.3) on the main street of Jalan Ipoh Kampar (the center of the map) where the traffic is affected by the street flooding 1 to 2 times every year. The second area is New Wah Loong which is the residential area located at the southwest part of the map. The flood in New Wah Loong is mainly due to the capacity of the bed of Sungai Keranji not deep enough to drain

Fig.3 Observation of Kampar Flash Flood Event on 8 March 2022.

the water coming from the mountains down steep slopes near Hospital Kampar (center of the map in Fig.3). This causes the overflowed river flooding into the outlet drain on Jalan 4 and into the low-lying area of New Wah Long. According to the villagers, the river water level will rise nearly 1m in less than 30 minutes and recedes after 2 hours.

Flood events were observed by the present authors in March 2022 and photos around the first hotspot near Maybank Kampar and those near New Wah Long were taken and shown in Fig.3. The rainfall started at about 4:10pm. The sequence of photos show how the runoff and flooding took place in about 20 minutes after the rain started. The rainfall intensity is estimated to be about 50mm/h at the first 20minutes and reduced gradually and stopped by 4:30pm. The location involved in the flash flood is mainly along Jalan Ampang, Jalan Masjid, Jalan Persekutuan Ipoh Kampar, 36 Food Court, Jalan 3 and Jalan 5 of New Wah Loong. Jalan Ampang, Jalan Masjid and Federal Road Ipoh Kampar also were all seriously flooded. The drains at the small village located at the eastern end of Jalan Ampang was almost full of runoff although it is wide and deep. Stormwater was collected from this village and Taman Golden Dragan and sent westward to natural retention pond through the major drains along Jalan Ampang, Jalan Masjid and Jalan Persekutuan Ipoh Kampar. 10min after the start of the rainfall, the overflow in front of Maybank Kampar, Jalan Ampang and Jalan Masjid started to occur including the back lane. The drain is filled with the brown water with sediments transported from the hill. From the observation, the final discharge outlets of the drainage system into the retention pond were not submerged and just the inlet and upstream are flooded. It shows that the existing drain capacity is not sufficient to convey the peak runoff flow from the hill during high intensity storm. Some parts of Jalan Ipoh Kampar were also hit by heavy rain causing the traffic jam in front of Maybank Kampar. The present runoff simulation is targeted to reproduce some of these flash flood events.

4. SIMULATION AND RESULTS

4.1 Simulation conditions

The view of the simulation area looking east (which is different from the map of Fig.2) is shown in the satellite image of Fig.4(a). The corresponding numerical model of the terrain represented by the boundary particles spaced at 2m interval (the total of 0.75 million particles) that include the roads and the buildings is shown in Fig.4(b) with color indicating the elevation. The rectangular coordinates are set so that x direction is from east to west, y vertically upward and z from south to north. The surface runoff from the mountain slopes flows mainly through the urban area and into a retention pond (blue area near bottom center of Fig.4(b)). The simulation is mainly the overland flow in the area 1.5km east to west by 2.0km north to south. The rain is simulated by lumps of water of volume 1m^3 each and placed at intervals of 80m near the ground elevation as shown in black dots in Fig.4(b). 475 rain particles are introduced at one time. The positions of introducing the rain particles are varied in time and the volume of the rain particles and the frequency of introducing rain particles are adjusted so that they correspond to the rainfall intensity of 80mm/h. The rainfall intensity is assumed constant through the simulation period and is a little more intense than that observed in March 2022. The simulation calculation is run on a workstation consisting of Intel 3.8GHz Xeon Gold 5222. The simulation computation for 30 minute rainfall runoff took about 2 weeks of computation time.

The main objective in the present simulation is to find if the characteristics of the runoff and urban flash floods like that observed in March 2022 can be reproduced. Therefore, the runoff simulation was conducted for rainfall of 80mm/h for 30 minutes. The surface roughness height k is set to 1m in mountain areas with trees, while those for the natural ground without trees, paved surfaces and building surfaces are set as 0.5m, 0.1m and 0, respectively. Although the present model allows initial abstraction and the infiltration depending on the ground conditions, the infiltration and the subsurface flow are neglected. The ground infiltration delays the overland flow but the runoff due to sudden tropical rain storm takes place suddenly and the effects of the slow infiltration and the subsurface flow are expected to be small.

The two areas where street inundation occurs frequently are indicated by circles in Fig. 4(a).

(a) Google satellite image of the simulation area (b) Numerical representation of the simulation area

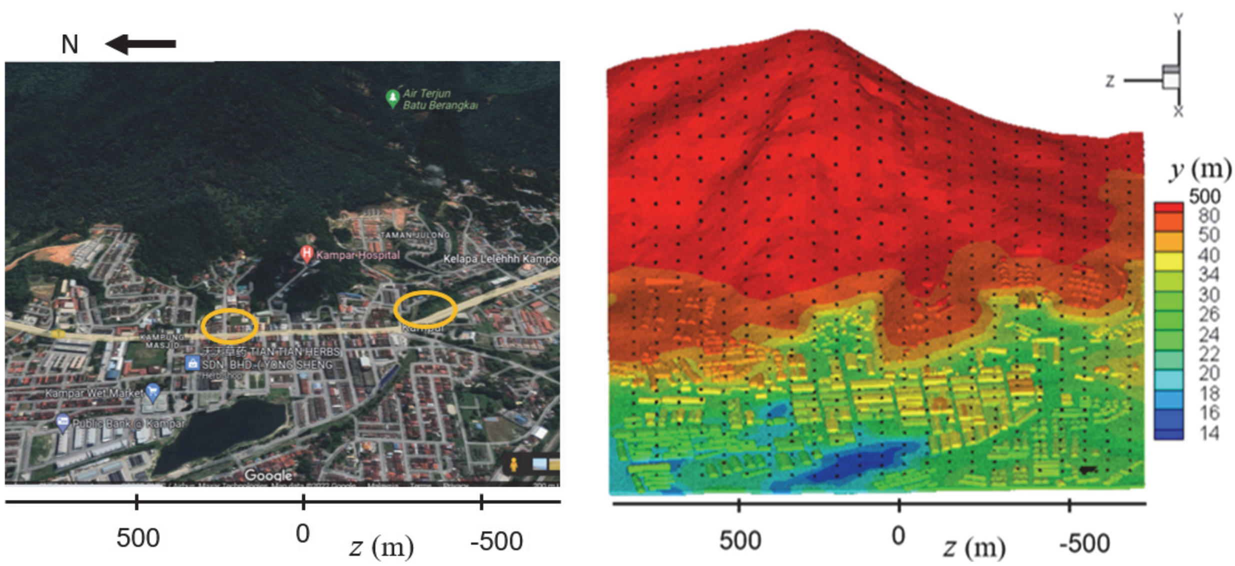

Fig.4 Simulation area and the numerical model.

4.2 Simulation results

Fig. 5 shows the distribution and movement of the surface water represented by rain particles on the ground, at 6 minutes (Fig.5(a)) and at 25 minutes (Fig.5(b)) after the start of rainfall. The black dots indicate the rain particles. Each dot corresponds to a lump of water with the volume corresponding to 1m^3. In practice this volume is spread flat on the ground initially but as the volume of water gets collected, they interact each other forming large body of water. It is seen that due to the sudden rain of strong intensity, the overland flow pattern develops very quickly. This is the feature of the runoff in this region with tropical rainstorms. The flow paths are seen to depend strongly on the topographical characteristics and tend to follow small valleys. The surface flow then appears to collect to certain locations at the foot of the mountain slopes that correspond closely to the frequently flooded hot spots.

The runoff is accelerating as it travels down the steep hill slope to the lower elevation area. Until it reaches the town area, the runoff from the hill is slowed down by the residential houses situated at the foot of the hill. The flow direction and velocity of the runoff from the hill are determine by the topological feature of the terrain including the friction. Much of the rainwater in the simulation area drains into the small lake located at the lower center. The lake works as a retention pond, and it flows out to the small river (Keranji River) flowing near the west (lower) border of the simulated region.

Few minutes after the start of the rain, three major waterways are formed as a results of water flow from the hill. The constructed new residential houses on Taman Golden Dragon (near the top of the map in Fig. 3 and indicated by TGD in Fig. 5) have redirected the runoff towards the village located at the east end of Jalan Ampang as shown in Fig. 5. Due to the rising elevation of Kampar Hospital (center of the map in Fig. 3, and indicated by KH in Fig.5), the runoff from the hill is divided into the villages located at both north and south parts of Kampar Hospital. This results in a total of two water paths from Taman Golden Dragon and Kampar Hospital is flow towards the village located at the end of Jalan Ampang eventually accumulating in this small valley. This village has a lower elevation compared to the surrounding terrain, so it forms a bowl geometry and collecting runoff directly from the steep mountain. As seen in Fig.5(b), another water paths toward the south of Kampar Hospital creates another patch of water.

In order to examine the water movement and accumulation in detail, three subareas Area A, Area B and Area C shown in

(a) 6 minutes after start of rain (b) 25 minutes after start of rain

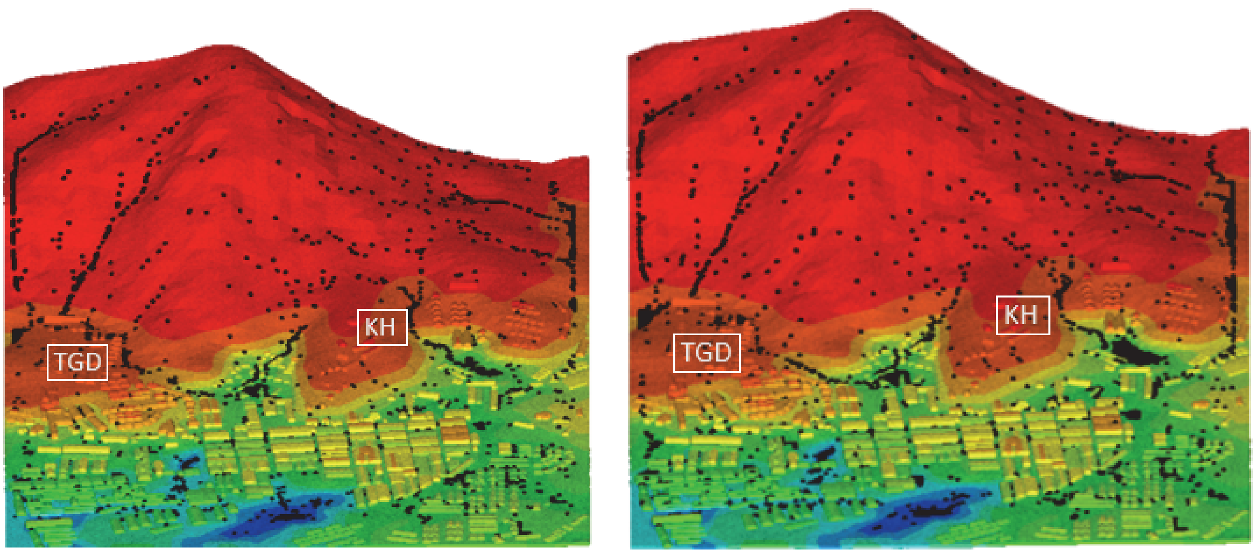

Fig.5 Distribution of surface water represented by particles after rainfall. The color scale representing the elevation is the same as in Fig.4 and the black dots indicate rain particles. Taman Golden Dragon is indicated by TGD and Kampar Hospital is indicated by KH.

Fig.6 are chosen. The close-up view of the surface water between Taman Golden Dragon and Hospital Kampar are shown in Fig.7. The color of water particles indicates the pressure. 10KPa corresponds to hydrostatic pressure of about 1m deep water. The stream of surface water is seen to come down from the mountain and gathers at the foot of the slope. This is a few blocks east of the Hotspot A on Jalan Ipoh Kamar. At *t*=6 min small patch of water is seen there and at t=20min, the pressure is about 8kPa and the depth of water is reaching 1m. The patches of water collected along some buildings after *t*=10 min. seem to correspond to street flooding seen in the photos Fig.3 (d) and (e) taken at 4:12.

Fig.8 shows similar accumulation of water in Area B south of Kampar Hospital. The water depth there is seen to increase more than 0.5m and over some area. This water does flow into Keranji River but the water seems to stagnate and inundate the area in short time. In the observation shown in Fig.3, no photos were taken in the area between Kampar Hospital and Keranji River but this area has been known to be flooded frequently.

The overland flow in the urban area depends not only on the ground topography but on the layout of blocks and buildings. Fig.9 shows the water particles in Area C in New Wah Loong. Though the depth indicated by the pressure is small, there are areas with quite large patches of collected water. Some rainwater falling on the sloping rooftop drains directly to the ground and to the lower elevation region. Some makes their way into the natural retention pond and Sungai Keranji but some gets gathered in the low-lying areas, particularly Jalan 2 and 3 in New Wah Loong. This corresponds to photos (h), (i) and (j) in Fig.3 which show inundation of the streets by the buildings.

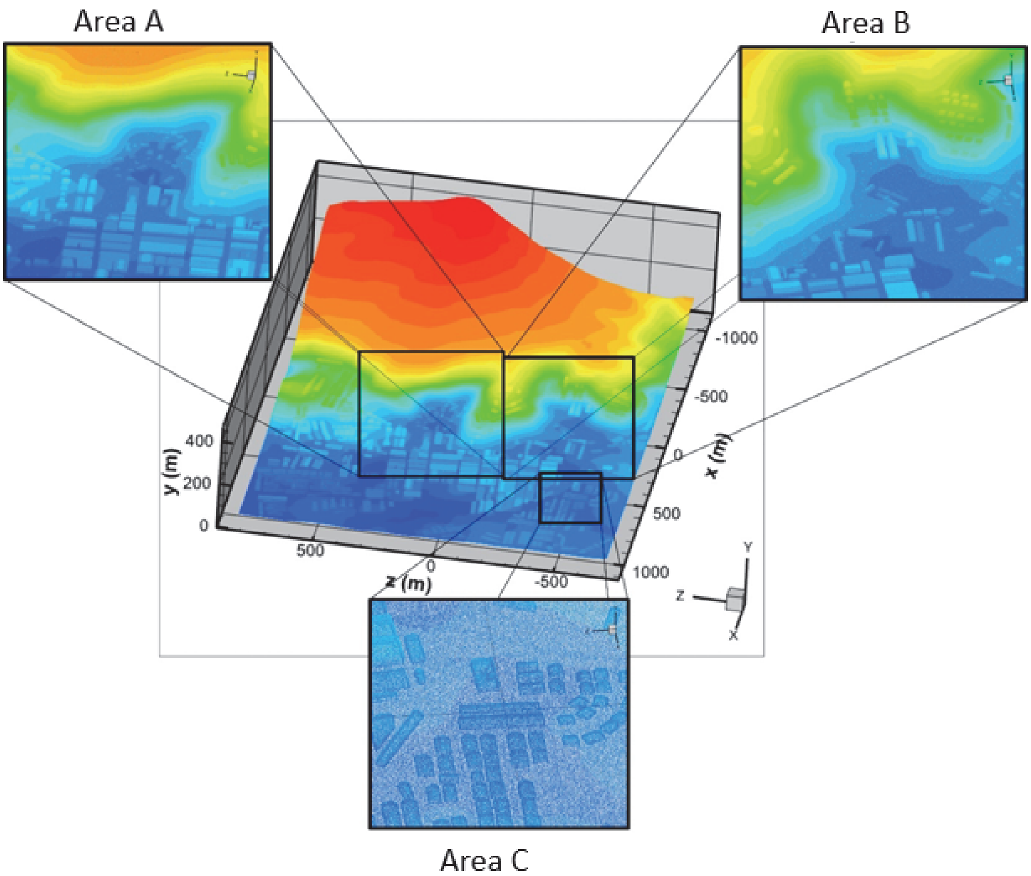

Fig.6 Locations of areas for detailed examination.

(a) t=6 min. (b) t=10min. (c) t=20 min,

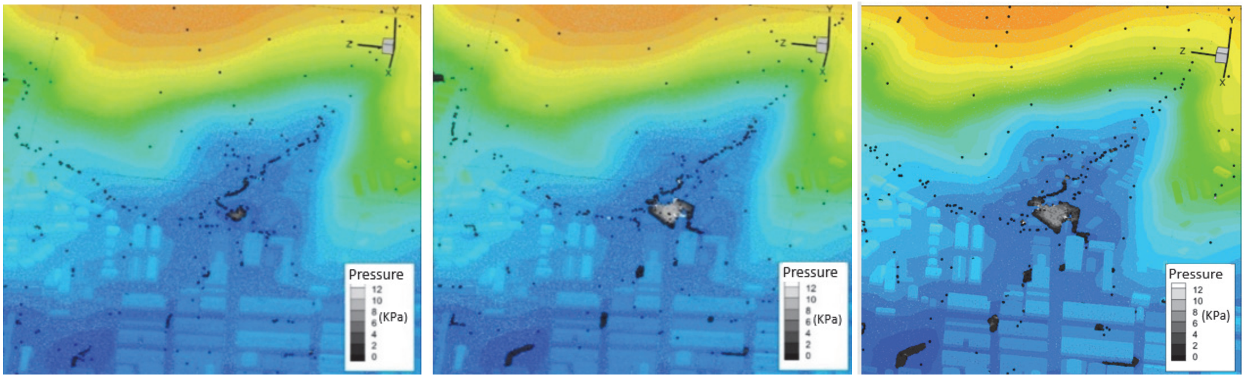

Fig. 7 Surface flow and inundation in Area A between Taman Golden Dragon and Hospital Kampar, the gray scale indicates pressure in KPa

(a) t=6 min. (b) t=10min. (c) t=20 min,

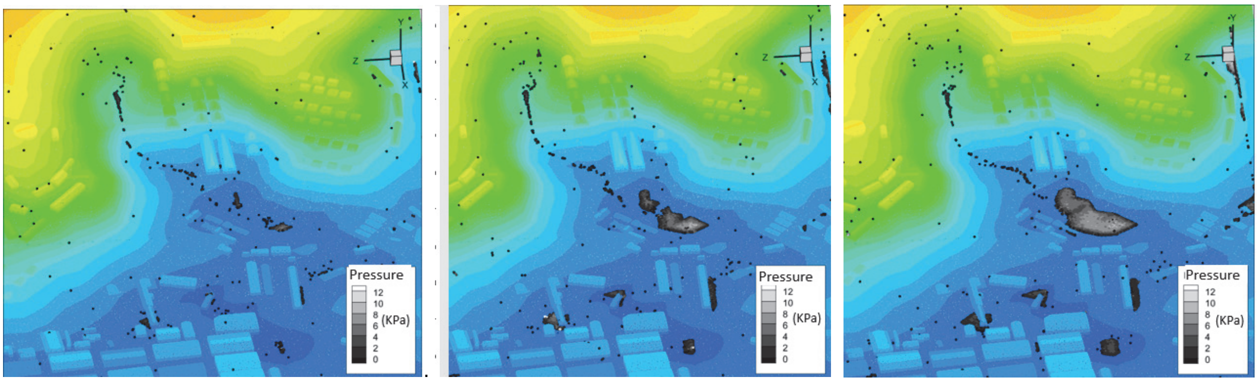

Fig. 8 Surface flow and inundation in Area B south of Kampar Hospital, the gray scale indicates pressure in KPa.

(a) t=6 min. (b) t=10min. (c) t=20 min,

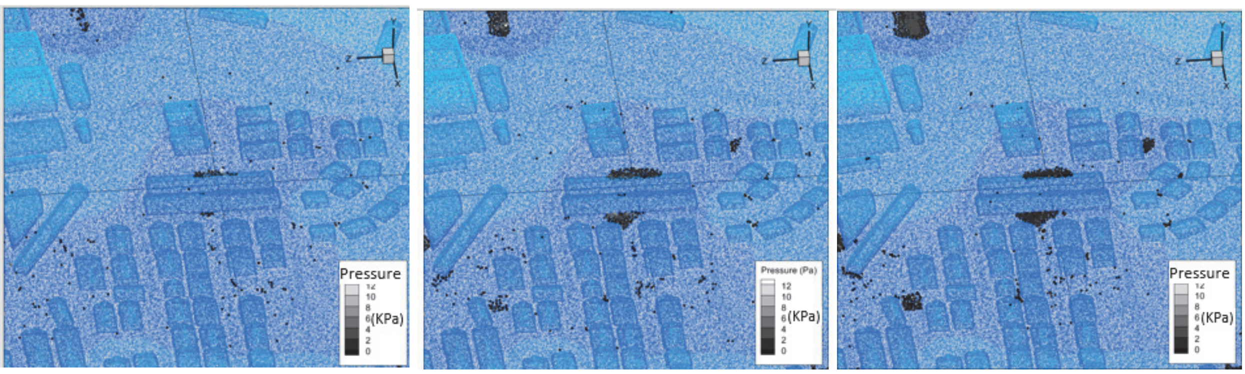

Fig. 9 Surface water in Area C in New Wah Loong area, the gray scale indicates pressure in KPa.

5. CONCLUSION

The three-dimensional weakly compressible smoothed particle hydrodynamics (WCSPH) has been applied to the simulation of the direct runoff and the overland flow due to rainfall. It is applied to a small catchment area of 1.5km x 2km near a mountain in the town of Kampar, Perak, Malaysia. The targeted rainfall and flood events that were observed in March 2022 were simulated. The pattern of the surface water distribution in a complex real mountainous topography appears to match the observation at the simulated site. The simulation result represents important features of the observed flood events. The results do have limitation that the smallest volume of water is $1m^3$, but the resolution can be improved if a computer with larger power is used. Although the present method has not been evaluated and directly compared with the existing inundation prediction methods, it can be a new method that directly simulates the overland flow and inundation due to rainfall in mountainous and urban terrains including structures. The subsurface water has totally been ignored but the model allows the effects of the subsurface flow to be included for longer duration events.

ACKNOWLEDGEMENT

The present work was partly supported by Universiti Tunku Abdul Rahman Research Fund UTARRF/2022-C1/A03 and Malaysian Ministry of Higher Education Fundamental Research Grant System FRGS/1/2019/TK01/UTAR/01/1.

REFERENCES

1) Sitter son, J., Knightes, C., Parmar, R., Wolfe, K., Muche, M. and Avant, B.: *An overview of rainfall-runoff model types*. Athens: Unites States Environmental Protection Agency, 2017.

2) Gayathri, K.D., Ganasri, B.P., and Dwarakish, G.S.: A Review on Hydrological Models *Aquatic Procedia*, 4, pp.1001–1007. http://dx.doi.org/ 10.1016/j.aqpro.2015.02.126, 2015.

3) Kokkonen, T., Koivusalo, H. and Karvonen, T.: A semi-distributed approach to rainfall-runoff modelling—a case study in a snow affected catchment. *Environmental Modelling & Software*, 16(5), pp.481-493, 2001. http://dx.doi.org/10.1016/S1364-8152(01)00028-7

4) Beven, K. J.: *Rainfall-runoff modelling: the primer*. (2nd ed.): Wiley-Blackwell, 2012.

5) United States Department of Agriculture: Natural Resources Conservation Service, part 630 Hydrology, National Engineering Handbook, 2004.

6) Zhang, W. and Cundy, T. W.: Modeling of two-dimensional overland flow, *Water Resourc. Res.*, Vol. 25, pp. 2019-2035, 1989.

7) Teng, J., Jakeman, A., Vaze, J., Croke, B. F., Dutta,, D. and Kim, S.: Flood inundation modelling: A review of methods, recent advances and uncertainty analysis, *J. Hydrol*., Vol. 315, pp. 220-235, 2005.

8) Li, X., Fang, X., Li, J., Manoj, K.C., Gong, Y. and Chen, G.: Estimating time of concentration for overland flow on pervious surfaces by particle tracking method, *Water MDPI*, Vol. 10, 379, 2018.

9) Jamaludin, S.S., Zin, Z.W.Z., Deni, S.M. and Jemain, A.A.: Trends in Peninsular Malaysia rainfall data during the southwest monsoon and northeast monsoon seasons: 1975–2004. Sains Malaysiana, 39(4), pp. 533–542, 2010.

10) Vacondio R., Rogers B. D., Stansby, P. K.: SPH modeling of shallow flow with open boundaries for practical flood simulation, *J. Hydraul. Eng*., Vol. 138(6), pp. 530–541, 2012.

11) Chang, T.-J., Chang, Y.-S. and Chang, K.-H.: Modeling rainfall-runoff processes using smoothed particle hydrodynamics with mass-varied particles, *J. Hydrol*., Vol. 543, pp. 749-758, 2016.

12) Fei, X., Yan, H., Tao, T., Xin, K. and Li, S.: Integrated rainfall-runoff process with shallow water model by mass varied smoothed particle hydrodynamics: Infiltration effect implementation, J. Hydrodynam.,Vol. 33, pp.1190-1201, 2021.

13) Monaghan, J. J. : Simulating free surface flows with SPH, *J. Comput. Phys*. Vol. 110. pp. 399-406, 1994.

14) Violeau, D. and Rogers, B. D.: Smoothed particle hydrodynamics (SPH) for free-surface flows: past, present and future, *J. Hydraul. Res.*, Vol. 54, No. 1, pp. 1-26, 2016.

15) Nakayama, A., Lye, X.Y. and Ng, K.C.: Wall-layer boundary condition method for laminar and turbulent flows in weakly compressible SPH, *Eur. J. of Mech. /B Fluids*, Vol. 95, pp. 276-288, 2022.

16) Lye, X.Y., Nakayama, A. and Tan, S.Y.: Simulation of overland flow due to rainfall using smoothed particle hydrodynamics, *Journal of Japan Society of Civil Engineers* Ser B (Hydraulic Engineering), accepted, 2022.

17) Majlis Daerah Kampar: Background of Kampar. [online] Available at: <https://ww.mdkampar.gov.my/en/visitors/background-kampar/page/0/2> [Accessed 22 August 2021]

AUTHORS

Tan Sin Ying Undergraduate student

Akihiko Nakayama Ph D. Fluid Mechanics, Hydraulics

Lye Xin Yan Graduate student B.S.